Environmental
Science
Nano

ROYAL SOCIETY
OF CHEMISTRY

PAPER

View Article Online
View Journal | View Issue

Check for updates

Cite this: *Environ. Sci.: Nano*, 2021, **8**, 784

Piezoelectric activation of peroxymonosulfate by MoS_2 nanoflowers for the enhanced degradation of aqueous organic pollutants†

Shuhui Liu,‡[a] Binghua Jing,‡[a] Chunyang Nie,[a] Zhimin Ao, *[a] Xiaoguang Duan, [b] Bo Lai, [c] Youyuan Shao,[d] Shaobin Wang [b] and Taicheng An [a]

Received 12th December 2020,
Accepted 9th February 2021

DOI: 10.1039/d0en01237h

rsc.li/es-nano

Natural mechanical energies, such as wind, tidal waves, and water flow, widely exist in the environment and these inexhaustible natural mechanical energies can be utilized through piezoelectric materials for the degradation of aqueous organic pollutants in the environment. In this work, few-layered molybdenum disulfide nanoflowers (MoS_2 NFs) were adopted as a piezocatalyst to activate peroxymonosulfate (PMS) with ultrasonic waves (US) as the mechanical force for phenol abatement. A much higher degradation efficiency was attained by the integrated US/MoS_2 NFs/PMS system compared to other single systems, revealing the markedly synergistic effect of US and MoS_2 on PMS activation. Moreover, density functional theory calculations were performed to fundamentally understand the charge distribution in a polarized MoS_2 nanosheet under different strains and to understand the piezocatalytic properties of MoS_2 nanosheets, as well as reaction pathways between PMS and carriers on the active edges of MoS_2 for the production of free radicals. It was found that both sulfate radicals ($SO_4^{\bullet-}$) and hydroxyl radicals ($^{\bullet}OH$) were produced in the US/MoS_2 NFs/PMS system. However, $SO_4^{\bullet-}$ was quickly converted into $^{\bullet}OH$ *via* a hydrolysis reaction under US, enabling $^{\bullet}OH$ to be the primary reactive oxygen species for phenol oxidation. This work offers an efficient piezocatalyst to activate persulfate for water remediation. More importantly, it provides fundamental insights into the piezoelectricity in two-dimensional semiconducting materials and the mechanism in the piezocatalytic activation of persulfate. Results prove that the combination of piezoelectricity and advanced oxidation processes is promising for water pollution control, and provides a new idea for the application of inexhaustible natural mechanical energy in the environment for environmental remediation.

Environmental significance

In the past few decades, persulfate-based advanced oxidation processes (PS-AOPs) in abating aqueous organic pollutants have attracted widespread interest. However, the high energy consumption and poor stability of catalysts have hindered their wide-spread practical application. Therefore, it is of great significance to explore an energy-saving and reuse method to activate persulfate for decontaminating organic matter in advanced wastewater treatment. It is known that inexhaustible natural mechanical energy can be used for the degradation of organic pollutants by piezoelectric materials. In this study, we successfully used two-dimensional MoS_2 nanoflowers (MoS_2 NFs) as a piezoelectric material model for PMS activation and for the subsequent degradation of organic pollutants. Experimental results indicated that MoS_2 could significantly activate PMS under external force, whereby both sulfate radicals ($SO_4^{\bullet-}$) and hydroxyl radicals ($^{\bullet}OH$) were produced in the US/MoS_2 NFs/PMS system. The odd-numbered petals exposed at the edge of MoS_2 NFs provided favorable active sites for the occurrence of piezoelectric catalysis. For understanding the internal mechanism of 2D piezoelectric materials for catalyzing PMS activation process, density functional theory calculations (DFT) were performed to determine the piezocatalytic properties of MoS_2 nanosheets, as well as reaction pathways between PMS and carriers on the active edges of MoS_2 for free radical production. The outcomes of this study provide an effective piezocatalyst for water remediation, and also an insightful understanding of piezoelectricity in 2D materials and piezoelectric catalytic AOP.

---

[a] *Guangzhou Key Laboratory of Environmental Catalysis and Pollution Control, Guangdong Key Laboratory of Environmental Catalysis and Health Risk Control, School of Environmental Science and Engineering, Institute of Environmental Health and Pollution Control, Guangdong University of Technology, Guangzhou 51006, China. E-mail: zhimin.ao@gdut.edu.cn*

[b] *School of Chemical Engineering and Advanced Materials, University of Adelaide, Adelaide, SA 5005, Australia*

[c] *College of Architecture & Environment, Department of Environment Science & Engineering, Sichuan University, Chengdu 610065, Sichuan, China*

[d] *School of Chemical Engineering and Energy Technology, Dongguan University of Technology, Dongguan 523808, China*

† Electronic supplementary information (ESI) available. See DOI: 10.1039/d0en01237h

‡ These authors contributed equally to this work.

1. Introduction

Over last few decades, there has been broad interest in utilizing persulfate-based advanced oxidation processes (AOPs) for the abatement of refractory organic contaminants in aquatic environments by the generated diverse reactive oxygen species (ROS).[1] Persulfate activation can be stimulated by physical or chemical approaches mainly, including heat, ultrasound (US), ultraviolet (UV) irradiation, electricity,[2] and catalysis.[3–10] Albeit their effectiveness at activating persulfate, these methods have some limitations. For instance, heat- or electro-activated AOPs are normally energy intensive;[3,11] the performance of US is unsatisfactory;[4,12] the penetration of UV light into water, especially muddy wastewater, is limited.[3,13] Catalytic activation is the most popular method for persulfate activation due to its various benefits, such as simplicity, high efficiency, and low energy input. Metal-based and carbon-based materials are the most extensively used catalysts for persulfate activation; albeit they usually suffer from the drawback of low stability in long-term operation.[3,4,7,14,15] Therefore, exploring energy-saving and high-performance approaches to activate persulfate for decontaminating organics is of significance in advanced wastewater treatment.

The piezoelectric effect is described as a physical phenomenon whereby external mechanical vibrations cause the spontaneous polarization of piezoelectric materials due to structural deformation, giving rise to the formation of a built-in electric field.[16,17] Apart from its application in nanogenerators and self-powered nanosystems, the piezoelectric effect is also applied to drive chemical reactions, such as water splitting and the degradation of organic pollutants *via* piezocatalysis.[18,19] Piezocatalysis is quite analogous to the well-known photocatalysis. Here, the surface electron–hole pairs of strained piezoelectric crystals are charge carriers in the conduction and valence bands of photocatalysts to coordinate redox reactions.[20] Several works have shown that the photoinduced electrons and holes are able to react with persulfate to produce free radicals.[4,21] Very recently, Lan *et al.*[22] utilized $BaTiO_3$ as a piezocatalyst to activate peroxymonosulfate (PMS) under US vibration for degrading benzothiazole. They found that the US vibration could induce strains of $BaTiO_3$, and the resulting piezoelectric effect could effectively activate PMS to generate singlet oxygen for degrading organics, and an enhanced degradation performance was attained by the piezo-activated persulfate-AOP (PS-AOP) system as compared to piezocatalysis alone. Moreover, $BaTiO_3$ has shown good reusability in PMS activation. Thereby, piezoelectric catalysis is a promising energy-saving and reusable approach for persulfate activation.

Among the piezoelectric materials, inorganic ceramics like $Pb(Zr_{0.52}Ti_{0.48})O_3$ and $BaTiO_3$ are most favorable in chemical reactions due to their high piezoelectric properties.[23,24] Recently, two-dimensional (2D) piezoelectric materials have attracted great attention because of their higher crystallinity and greater tolerance of large elastic strains than those of conventional piezoelectric materials.[18,19] Also, 2D transition metal dichalcogenides, hexagonal boron nitride, *etc.* have been demonstrated to be piezoelectrics.[25,26] However, the applications of these 2D piezoelectric crystals in PS-AOPs have barely been explored. Meanwhile, due to the different piezoelectric properties and structures of 2D materials from $BaTiO_3$, there is some debate on the involved catalytic mechanism and reaction pathway in the piezocatalytic activation of persulfate processes and these still need to be fully ascertained. Particularly, the fundamental understanding of the piezoelectric behaviors of 2D materials is still lacking, and the evolution of ROS induced from the redox reactions between piezo-induced carriers and persulfate are also unambiguous. In addition, traditional piezoelectrics are mainly used in dye molecules, which can be more easily degraded compared with phenolic compounds. However, due to the developments in industry and agriculture, phenolic compounds, such as phenol, are widely released into wastewater and thus represent an important source of aqueous pollution in the environment, posing huge threats to human health and ecological systems, even at low concentrations.[27,28]

Herein, we adopted molybdenum disulfide nanoflowers (MoS_2 NFs) as a model 2D piezocatalyst to activate PMS for phenol (one of the most common toxic organic pollutants) degradation. The intrinsic mechanisms involved in the 2D piezoelectric material-catalyzed PMS activation process were investigated through both experiment and density functional theory (DFT) calculations. A radical-based reaction pathway was identified in the piezocatalytic PMS activation process *via* radical screening experiments and electron paramagnetic resonance (EPR). DFT calculations were conducted to elucidate the correlation between the piezoelectric polarization and the atomic orientation of MoS_2 nanosheets, the charge distribution in the polarized MoS_2 nanosheets under different strains induced by the US vibration, and the interactions between the PMS and the charge carriers on the active edges of MoS_2 for producing free radicals. Based on these results, we hope to offer an efficient method for activating persulfate to degrade aqueous toxic organic contaminants and also to deepen the understanding of piezoelectricity in 2D materials and piezo-catalyzed AOPs.

2. Materials and methods

Materials

Phenol was purchased from Aladdin Chemistry Co., Ltd. Potassium peroxymonosulfate (PMS, Oxone®) was supplied by Alfa Aesar Chemicals. Chromatographically pure methanol was provided by ANPEL Laboratory Technologies Inc. (Shanghai, China). 5,5-Dimethy-1-pyrroline-oxide (DMPO) was obtained from Sigma-Aldrich. Hydrochloric acid (HCl) was purchased from Guangzhou Chemical Reagent Factory. Sodium molybdate dihydrate ($Na_2MoO_4·2H_2O$, 99.95%, metal basis) was purchased from Shanghai Macklin Biochemical Co., Ltd. Thiourea was purchased from Tianjin Damao

Chemical Reagent Factory. Molybdenum sulfide (commercial MoS_2, 99.5%, metal basis, <2 μm) was supplied by Aladdin Biochemical Technology Co., Ltd. Ethanol (EtOH) was obtained from Tianjin Fuyu Fine Chemical Co., Ltd. *tert*-Butyl alcohol (TBA) was purchased from Shanghai Lingfeng Chemical Reagent Co., Ltd. All the regents were of analytical purity and used without any further purification. All solutions were prepared with ultrapure water of 18.25 mΩ cm.

Synthesis of MoS_2 NFs

A hydrothermal method was employed to synthesize MoS_2 NFs in this work, and the details of the synthesis can be found in Text S1.†

Material characterizations

X-ray diffraction (XRD) patterns were recorded with a Bruker D8-advanced X-ray diffractometer. The chemical states of elements in MoS_2 NFs were investigated by X-ray photoelectron spectroscopy (XPS, Thermo Escalab 250Xi) with Al-Kα X-ray. Raman spectroscopy (Horiba Jobin Yvon, LabRAM HR Evolution) was performed with an Ar+ laser of 532 nm. The morphology of the sample was observed by field emission scanning electron microscopy (SEM, LYRA 3 XMU, Tescan) and the structural details were further observed by field emission transmission electron microscopy (TEM, Talos F200S, FEI). The piezoelectric response of the material was measured by piezoresponse force microscopy (PFM, Dimension FastScan). Typically, MoS_2 NFs were directly loaded onto an ITO slice and to the top surface of the MoS_2 NFs a conductive atomic force microscopy (AFM) tip was applied at a specific compressive load to acquire its piezoelectric response potential.

Experimental procedures

The piezocatalytic property of the MoS_2 NFs toward PMS activation was evaluated by phenol oxidation. First, MoS_2 NFs (0.3 g L^{-1}) were dispersed in a phenol solution (10 mg L^{-1}) in a 100 mL glass beaker and stirred for 30 min in the dark at room temperature to establish the adsorption–desorption equilibrium between the MoS_2 NFs and the organic pollutant. Then, a certain amount of PMS (3.25 mM) was added into the suspension, and the mixture was quickly subjected to ultrasonic (US) vibration to initiate PMS activation. For comparison, control experiments, including phenol degradation by US-activated PMS alone and phenol degradation by MoS_2 NFs alone under US, were also conducted. The ultrasonic equipment was supplied by Kunshan Ultrasonic Instruments Co. Ltd (40 kHz, 300 W) and the temperature of the reaction suspension was kept around 25 °C during ultrasonication for all the experiments. At a predetermined time interval, an 0.8 mL aliquot was withdrawn from the reaction suspension and 0.2 mL ethanol was immediately injected into the aliquot to completely quench the oxidation reaction. Then the mixture was filtered into a high-performance liquid chromatography (HPLC) vial through a syringe filter with a polyether sulfone membrane of 0.22 μm pore size. Each experiment was performed in duplicate and the average values were adopted to ensure reproducibility.

Analytical methods

The concentration of phenol was measured by HPLC equipment with a UV detector (Elite, Eclassical3100) and a C-18 column (Waters). Methanol and ultrapure water were employed as the mobile phases at a flow rate of 0.8 mL min^{-1} and the wavelength of the detector was set at 270 nm. The solution pH was determined by a pH meter (Leici, Shanghai). EPR (Bruker, EMXplus-10/12) spectra were recorded to detect the generated free radicals during PMS activation and 5,5-dimethy-1-pyrroline-oxide (DMPO) was employed as the spin-trapping agent. The kinetics of the phenol degradation was analyzed by the pseudo-first-order kinetic model $\ln(C/C_0) = -k \times t$, where k is the first-order kinetic rate constant, and C and C_0 are the phenol concentrations at time t and $t = 0$, respectively. The dissolved Mo ions were detected using an inductively coupled plasma mass spectrometer (ICAP RQ, Thermo Fisher, Germany). Total organic carbon (TOC) was measured with a TOC analyzer (Shimadzu TOC-VCPH).

3. Results and discussion

Characterization of the MoS_2 NFs

Fig. 1a displays the morphology of the MoS_2 NFs as examined by SEM. The as-prepared sample was in the shape of NFs and

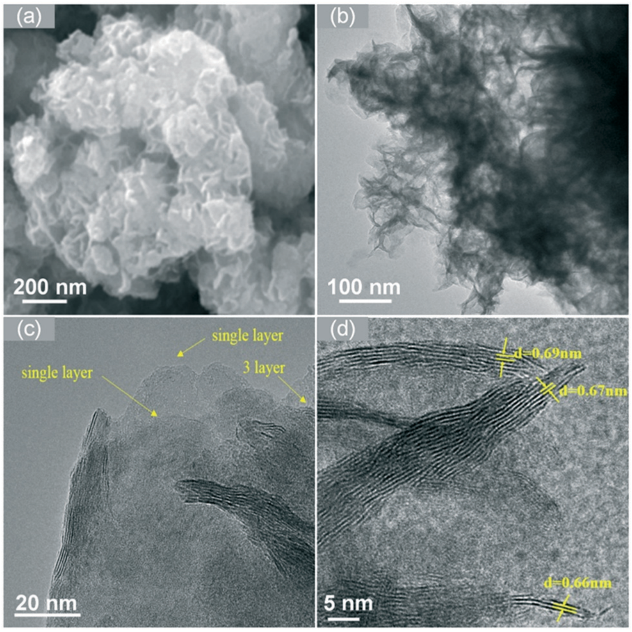

Fig. 1 (a) SEM images of the MoS_2 NFs morphology under high magnification; (b) low-magnitude TEM image of MoS_2 NFs; (c) HRTEM images of MoS_2 NFs showing the presence of single layers and few layers and (d) the measured lattice spacing for few-layered MoS_2 with different layer numbers at the edge of the MoS_2 NFs.

these NFs constituted a large number of nanopetals, which were beneficial for exposing more edges. In the TEM observation (Fig. 1b), it was found that each nanopetal was stacked by transparent nanosheets with a typical wrinkled and rippled structure. The microstructure of these nanosheets was further revealed by high-resolution TEM (HRTEM) images. Fig. 1c shows that some of the nanosheets were single-layered MoS_2 and the others were few-layered MoS_2, which is beneficial for exposing more active edge sites for inducing the piezoelectric polarization since only the MoS_2 with an odd number of layers is piezoelectric.[26] Meanwhile, the average lattice spacing in the few-layered MoS_2 was measured to be approximately 0.673 nm (Fig. 1d), consistent with the literature value of 0.67 nm.[29] According to the Bragg equation and the standard card of XRD, the lattice spacing shown in Fig. 1d corresponded to the (002) crystal plane of MoS_2. Moreover, XRD and Raman spectroscopy analyses were also conducted to characterize the structure of the MoS_2 NFs. It can be seen from Fig. 2a that all the characteristic peaks in the XRD pattern of the sample matched well with the reference powder diffraction file of MoS_2 (JCPDS No. 37-1492, 2H form). The peak of the (002) plane was slightly shifted to a lower scattering angle, due to the possibility that sodium ions and ammonium ions could be intercalated into the (002) layers of MoS_2 during the hydrothermal process.[30] Two characteristic peaks located at ~377 and ~403 cm^{-1} were observed in the Raman spectrum of the MoS_2 NFs (Fig. 2b), corresponding to the in-plane $E_{2g}{}^1$ and out-of-plane A_{1g} vibration modes.[29] Compared to the commercial bulk MoS_2, the Raman peaks of the two modes of the as-synthesized MoS_2 NFs were broader while the distance between them were shorter, suggesting the presence of single-layered and few-layered structures,[18,29,31] which is critical to inducing the piezoelectric effect of MoS_2.

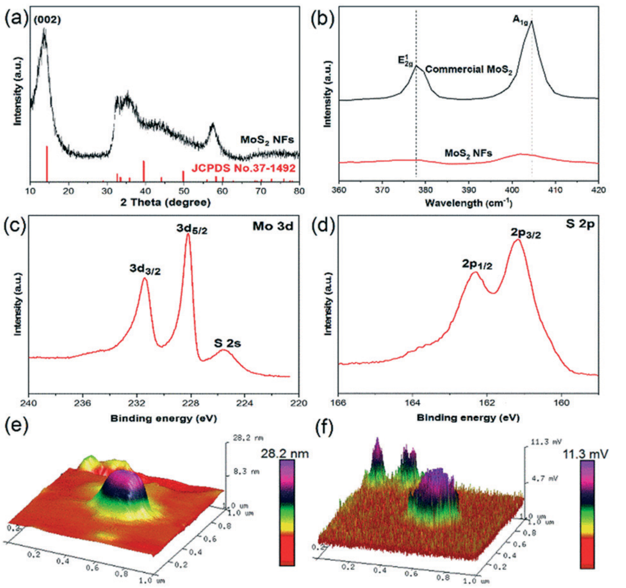

Fig. 2 (a) XRD pattern of MoS_2 NFs; (b) Raman spectra of MoS_2 NFs and commercial MoS_2; XPS spectra of (c) Mo 3d and (d) S 2p for MoS_2 NFs; (e) 3D topographic AFM image of MoS_2 NFs; (f) corresponding output piezoelectric potential of MoS_2 NFs.

The Mo 3d XPS spectrum of MoS_2 NFs is shown in Fig. 2c. The two peaks at 231.5 and 228.2 eV could be assigned to the Mo $3d_{3/2}$ and Mo $3d_{5/2}$, respectively, indicating that most of the Mo in the MoS_2 NFs existed as the Mo(IV) state.[32,33] The binding energies of the S 2p core-level of MoS_2 NFs (Fig. 2d) were split into two components ($2p_{1/2}$ and $2p_{3/2}$) located at 162.4 and 161.2 eV, respectively, originating from the spin–orbit coupling.[34] Through the above characterization, we proved that the synthesized material was indeed MoS_2 containing single- and few-layered structures, which are important for the piezoelectric effect.

For evaluation of the piezoelectric property of MoS_2 NFs, piezoresponse force microscopy (PFM) was performed. Fig. 2e shows the representative topography describing the detailed surfaces of the MoS_2 NFs, and the presence of the sample can be clearly seen from the convex part. The output of the corresponding 3D piezoelectric potential depicted in Fig. 2f provides evidences that the MoS_2 NFs indeed generated significant piezoelectric responses under external loading, indicating that the sample is a piezoelectric material. Especially, the highest value of the piezoelectric response prominently appeared at the edge active sites of the MoS_2 NFs, and the flower-shaped MoS_2 was conducive to exposing more edge positions, which was beneficial to the piezocatalytic activation of PMS.

Comparison of phenol degradation among various systems

US vibration has been reported to be able to provide sufficient mechanical strain to drive the deformation of piezoelectric crystals, generating polarized piezocatalysts for redox reactions.[19] Consequently, US vibration was imposed on the MoS_2 NFs to trigger the piezocatalytic activation of PMS toward phenol degradation in this work. To understand the contributions of activated PMS by US alone (US/PMS)[35,36] and the piezoelectric effect alone (US/MoS_2 NFs)[20,23] on the degradation of organic pollutants, we also carried out control experiments.

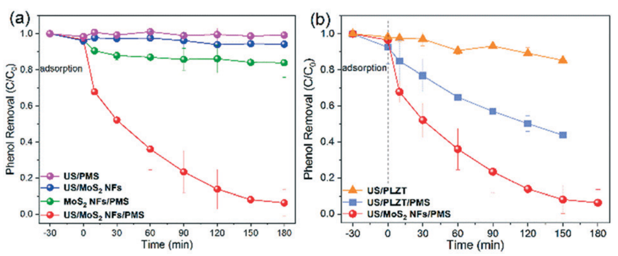

Fig. 3 (a) Phenol degradation by different systems: US/MoS_2 NFs/PMS, US/PMS, US/MoS_2 NFs, and MoS_2 NFs/PMS; (b) degradation efficiency of different piezoelectric materials: PLZT and MoS_2 NFs for phenol under US vibration. Conditions: [PMS] = 3.25 mM, $[phenol]_0$ = 10 ppm, $[MoS_2\ NFs]_0$ = 0.3 g L^{-1}, $[PLZT]_0$ = 5.0 g L^{-1}, US power = 300 W, temperature = 25 °C.

Fig. 3a depicts the phenol removal by various systems. Apparently, the MoS_2 NFs exhibited a poor adsorption of phenol and reached adsorption equilibrium within 30 min. After initiating the US vibration, phenol was degraded slowly by the US/PMS and US/MoS_2 NFs systems. Regarding the US/MoS_2 NFs system, ~10% of phenol was removed by sonication after 180 min, indicating that the as-prepared MoS_2 NFs indeed exhibit piezoelectricity under the sonic vibration but it was not really sufficient for direct phenol oxidation. In contrast, a rapid degradation of phenol was manifested by the US/MoS_2 NFs/PMS system and around 95% of phenol was removed after 180 min sonication; this efficiency was much higher than that of the US/PMS and US/MoS_2 NFs systems, indicating that the mechanical vibration imposed by the ultrasonication indeed induced the piezoelectric effect on the surface of the MoS_2 NFs, which activated persulfate for the degradation of organic pollutants. Recently, commercial bulk MoS_2 has been reported to be able to serve as a metal-based catalyst for PMS activation to degrade organic pollutants.[37,38] To understand the contribution of the intrinsic catalytic activity of MoS_2 NFs to phenol oxidation in the US/MoS_2 NFs/PMS system, the removal efficiency of phenol by MoS_2 NFs-catalyzed PMS activation without US vibration (MoS_2 NFs/PMS) was also assessed. It was observed that merely 17% of phenol was removed by the MoS_2 NFs/PMS system. We suspect that the degradation resulted from the MoS_2 NFs itself as a catalyst *via* the redox activation of Mo ions to activate persulfate. In the pseudo-first-order kinetic fitting, the rate constants (k) for the US/PMS, US/MoS_2 NFs, MoS_2 NFs/PMS, and US/MoS_2 NFs/PMS systems were calculated to be 0.00007, 0.00007, 0.00108, and 0.01961 min^{-1}, respectively (Fig. S1†). Apparently, the k value of the US/MoS_2 NFs/PMS system was about 16.07 times higher than the sum of the other three systems, revealing the significant synergistic effect of piezoelectric catalysis in PMS activation on the degradation of pollutants, sonication, and MoS_2-based catalysis on PMS activation. Therefore, we concluded that the remarkably enhanced phenol degradation performance of the US/MoS_2 NFs/PMS system could be attributed to the synergies between piezocatalysis and heterogeneous catalysis, and the piezoelectric effect was more efficient for PMS activation than for phenol degradation.

It is also reported that magnetic stirring is able to deform piezoelectric materials to induce piezoelectric effects, although it imposes a much lower mechanical strain than US vibration.[23] Therefore, the capacity of the piezoelectric effect for PMS activation was further consolidated by testing the degradation performances of the MoS_2 NFs/PMS system under magnetic stirring (ms) with different stirring rates (ms/MoS_2 NFs/PMS system) in our control experiments. It can be seen from Fig. S2† that the application of magnetic stirring on the MoS_2 NFs/PMS system indeed promoted the phenol degradation. The degradation efficiency increased gradually with the increased stirring rate, and a higher stirring rate led to a larger degree of deformation of the MoS_2 NFs, thus producing more polarized surface charge to activate PMS. However, the highest degradation efficiency reached by ms/MoS_2 NFs/PMS system (25%) was still much lower compared to the US/MoS_2 NFs/PMS system. We suspect that the piezocatalyst requires stronger mechanical vibration (US) for PMS activation.

Additionally, to explore whether the promoted phenol degradation efficiency in the US/MoS_2 NFs/PMS system was induced by the enhanced mass transfer under the US condition, we performed control experiments by using non-piezoelectric material carbon nanotubes (CNTs) as the PMS activator. As displayed in Fig. S3,† the degradation performances of the CNTs-driven PMS activation under US vibration (US/CNTs/PMS) and magnetic stirring (ms/CNTs/PMS) were quite identical, suggesting that the mass transfer effect made little contribution to the increased phenol degradation efficiency of phenol in the US/MoS_2 NFs/PMS system. This phenomenon also supported that the piezoelectric effect under US vibration could activate PMS to produce ROS for the efficient elimination of organic pollutants.

For comparison, we also tested the piezocatalytic performance for PMS activation by lanthanide lead zirconate titanate (PLZT), which is a commonly used piezoelectric crystal. As shown in Fig. 3b, a phenol degradation efficiency of around 56% was attained by the US/PLZT/PMS system within 150 min, which was much lower than that by the US/MoS_2 NFs/PMS system, even though the dosage of PLZT (5.0 g L^{-1}) was higher than MoS_2 NFs (0.3 g L^{-1}). This result indicated the superiority of MoS_2 NFs over PLZT as a piezocatalyst for PMS activation, and may be applied as an efficient piezoelectric catalyst in the advanced oxidation method for organics remediation.

Meanwhile, to evaluate the application potential of MoS_2 NFs in actual wastewater treatment, the phenol degradation efficiency of the US/MoS_2 NFs/PMS system in tap water was assessed. As shown in Fig. S4,† the removal rate of phenol in tap water was reduced to 54% within 180 min. This may be attributed to the presence of chloride ions and some other inorganic ions and natural organic substances in tap water, which are reported to be able to compete with organic pollutants for reacting with $^{\bullet}OH$ to produce species possessing a lower oxidative ability than $^{\bullet}OH$, resulting in a decline in degradation efficiency.[39,40]

Identification of the radical-based reaction pathway in the US/MoS_2 NFs/PMS system

To discern the primary ROS responsible for phenol oxidation by the US/MoS_2 NFs/PMS system, radical scavenging experiments with ethanol and *tert*-butyl alcohol (TBA) were conducted. Ethanol is generally used to screen both $^{\bullet}OH$ and $SO_4^{\bullet-}$ due to its high reaction rates with them ($k_{SO_4^{\bullet-}}$ = 1.6–7.7 × 10^7 M^{-1} s^{-1}, $k_{\cdot OH}$ = 1.2–2.8 × 10^9 M^{-1} s^{-1}),[4,41] while TBA is a specific radical scavenger for $^{\bullet}OH$ due to its much higher reaction rate with $^{\bullet}OH$ ($k_{\cdot OH}$ = 3.8–7.6 × 10^8 M^{-1} s^{-1}) than

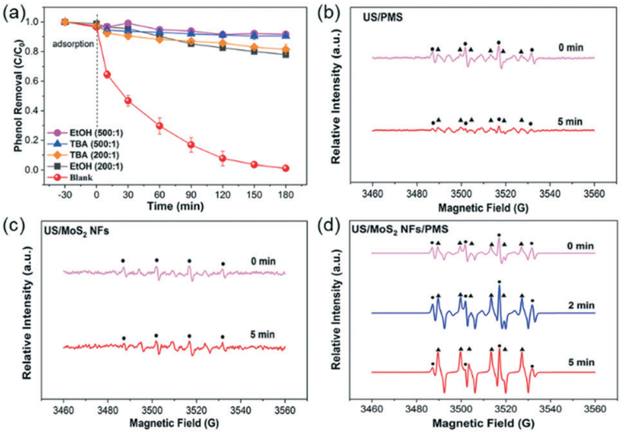

Fig. 4 (a) Phenol degradation in the US/MoS$_2$ NFs/PMS system with addition different ratios of ethanol and TBA. EPR spectra of free radicals in different experimental systems (b) US/PMS, (c) US/MoS$_2$ NFs, (d) US/MoS$_2$ NFs/PMS, (▲: DMPO$^{\bullet}$–SO$_4^-$, ●: DMPO$^{\bullet}$–OH). Conditions: [PMS] = 3.25 mM, [phenol]$_0$ = 10 ppm, [MoS$_2$ NFs]$_0$ = 0.3 g L^{-1}, US power = 300 W, temperature = 25 °C.

$SO_4^{\bullet-}$ ($k_{SO_4^{\bullet-}}$ = 4–9.1 × 10^5 M^{-1} s^{-1}).[42] Fig. 4a displays phenol degradation by the US/MoS$_2$ NFs/PMS system in the presence of different amounts of ethanol or TBA. Phenol oxidation was greatly inhibited when the molar ratio of ethanol and PMS was 200 : 1, while a further increase of the molar ratio to 500 : 1 resulted in a nearly complete inhibition. Surprisingly, the addition of TBA with the same doses as ethanol exerted equivalent inhibitory effects on phenol degradation. These results indicated that $^{\bullet}$OH was generated from the US/MoS$_2$ NFs/PMS system and dominated the oxidation of organics, differing from the nonradical US/BaTiO$_3$/PMS system.[22]

In principle, external energy is supplied to activate and cleave the peroxide O–O bond in PMS to produce ROS, such as $SO_4^{\bullet-}$ or $^{\bullet}$OH.[3,43] However, the production of $SO_4^{\bullet-}$ over the US/MoS$_2$ NFs/PMS system was not proven on the basis of the quenching experiments. It has been documented in the literature that $SO_4^{\bullet-}$ would be quickly transformed into $^{\bullet}$OH *via* an hydrolysis reaction in the hot interfacial region of the cavitation bubbles formed from US.[44] We suspect that $SO_4^{\bullet-}$ would be quickly hydrolyzed under the action of ultrasound to produce $^{\bullet}$OH at a rate much greater than the rate at which ethanol and $SO_4^{\bullet-}$ combine. On these grounds, we speculated that $SO_4^{\bullet-}$ was also initially produced from the piezocatalytic activation of PMS over MoS$_2$ NFs in the US/MoS$_2$ NFs/PMS system, and the resulting radicals were subsequently transformed into $^{\bullet}$OH very quickly under the US vibration to attack the organic pollutants.

To verify this assumption, the EPR spin-trapping technique was employed using DMPO as a spin trap to capture short-lived free radicals in aqueous solution. As shown in Fig. 4b, weak signals corresponding to the DMPO$^{\bullet}$–OH and DMPO$^{\bullet}$–SO$_4^-$ adducts were detected in the PMS solution, which could be assigned to the hydrolysis of PMS. The intensity of the two signals barely increased upon sonication, indicating that negligible amounts of $SO_4^{\bullet-}$ and $^{\bullet}$OH were derived from the US/PMS system, which accounted for the poor degradation performance of the US/PMS system. As for the US/MoS$_2$ NFs system (Fig. 4c), a slight increase in the intensity of the DMPO$^{\bullet}$–OH signal was observed after sonicating the MoS$_2$ NFs suspension. This suggested a limited capacity of the piezoelectric MoS$_2$ NFs for oxidizing H$_2$O into $^{\bullet}$OH, which agreed with the low phenol degradation efficiency of the US/MoS$_2$ NFs system. Fig. 4d illustrates the EPR signals for the US/MoS$_2$ NFs/PMS system. The signals of the DMPO$^{\bullet}$–OH and DMPO$^{\bullet}$–SO$_4^-$ adducts were enhanced after adding the MoS$_2$ NFs into the PMS solution, stemming from the PMS activation by MoS$_2$ NFs itself. Upon applying US vibration on the MoS$_2$ NFs/PMS system, the intensity of the two signals increased significantly in 2 min, suggesting the effective piezocatalytic activation of PMS to generate both $SO_4^{\bullet-}$ and $^{\bullet}$OH. Notably, after 5 min US treatment, the intensity of the DMPO$^{\bullet}$–SO$_4^-$ adduct further increased, but the intensity of the DMPO$^{\bullet}$–OH adduct declined slightly, demonstrating the conversion of $SO_4^{\bullet-}$ to $^{\bullet}$OH. This fact supports the hypothesis that the piezocatalytic activation of PMS over MoS$_2$ NFs primarily produces $SO_4^{\bullet-}$, and this radical then evolves into other ROS under ultrasonication during the degradation process.

Theoretical investigation of the mechanism for the piezocatalytic activation of PMS over the MoS$_2$ NFs

Although the above results indicated that the ROS in the US/MoS$_2$ NFs/PMS system were $^{\bullet}$OH and $SO_4^{\bullet-}$, the conversion process between them is still unknown. To this end, DFT calculations were employed to clarify the reactions occurring on the surface of the single- and few-layered MoS$_2$ NFs. Details of the modeling are provided in the ESI† (Text S2). The favorable structure of MoS$_2$ is shown in Fig. S5a.† The piezoelectricity of MoS$_2$ with tensile and compressive strains along the "zigzag", "armchair", and biaxial directions were investigated in this work, aiming to take all the possible situations into consideration for the strains induced by the US in experiments. The strengths of uniaxial strains along each direction were set as −10%, −5%, 0, +5%, and +10%, respectively. Zero means MoS$_2$ without strain; "−" refers to the compressive strain; and "+" refers to the tensile strain.

For piezoelectric materials, the magnitude of the dipole moment has a certain relationship with the piezoelectric strength. Therefore, the specific dipole moments of MoS$_2$ under the applications of different uniaxial strains were calculated, and the detailed information is listed in Text S3.† The biaxial strain had little effect on the dipole moment, so the situation of biaxial strain will not be discussed much in this work. Only the strains along the "zigzag" direction were considered in the following DFT calculations for the piezocatalytic activation of PMS due to the similar effect of the strains along the "zigzag" or "armchair" directions. Strain caused the in-plane polarization of MoS$_2$ to form an internal electric field, which made the free charge move directionally. As displayed in Fig. S7a,† compared with the pristine MoS$_2$, the in-plane polarization of MoS_2 was generated upon imposing a uniaxial strain ("armchair" or "zigzag"), stemming from its noncentrosymmetric structure. Fig. S7b and c† show that polarized charges (electrons e^- and holes h^+) appeared at the surface of MoS_2 under tensile or compressive strains, producing an internal electric field, and this electric field could drive the flow of free charges within the piezocrystal, producing an electric current. This phenomenon is widely applied to fabricate piezoelectric effect-based nanogenerators and flexible self-powered systems, for accomplishing the conversion from mechanical to electric energy.[45,46] In addition, the movement of the free charges (piezo-induced e^- and h^+) to the surface of the polarized piezocrystal can also react with the surrounding medium to initiate the piezocatalysis.[31]

Table S1† depicts the atomic charges of single Mo and S atoms under various strains. The atomic charges of Mo and S atoms under "armchair" strains were equivalent to those under "zigzag" strains with the same strain strength, while the charge changes with the uniaxial strains were less than those with biaxial strains. The change in atomic charges in the strained MoS_2 was ascribed the exertion of both uniaxial and biaxial strains inducing a deformation of the charge density, leading to the suppression of the repulsion interactions between bonding states in the valence band and antibonding states in the conduction band. Since the electron–hole separation caused by the piezoelectric effect is similar to in the photocatalytic process, we calculated the band structures of MoS_2 under different strains. The band structures and specific parameters of all the configurations are shown in Fig. S8 and Table S2.† We found that the band gap of MoS_2 declined with the increase in tensile strain for both biaxial and uniaxial strains. However, when both biaxial and uniaxial compressive strains were applied, the band gap of MoS_2 increased slightly at −5% strain, and then decreased with the increase in strain strength to −10%. Thus, the band gap had an optimal range. The effect of HSO_5^- activation on MoS_2 with −10% strain may be more significant than that of −5% strain. The decrease of the bandgap in MoS_2 increased the possibility of the electrons being transport from the valence band to the conduction band, thus improving the generation of electron–hole pairs, which is beneficial to the piezoelectric catalysis.[47] Therefore, the above calculations theoretically consolidated the finding that MoS_2 can exhibit a piezoelectric effect under US vibration, as found in the experiments. The change in energy band demonstrated that MoS_2 under strain is more conducive to the separation of electrons and holes, thereby promoting persulfate activation. Thus, the degradation efficiency in the US/MoS_2 NFs/PMS system was much higher than in the other systems, as found in the above experiments.

Then the interaction between PMS and polarized MoS_2 was studied to illustrate the evolution of free radicals in the US/MoS_2 NFs/PMS system. In the case of polarized MoS_2, both the adsorption of HSO_5^- onto the edges accumulated with piezo-induced e (e_{piezo}, compressive strain) and piezo-induced h^+ (h^{+}_{piezo}, tensile strain) were considered. In addition, the MoS_2 shown in Fig. S9† was used as the substrate in the activation reaction, because it not only had the same and enough surface for the reaction with HSO_5^-, but also allowed saving computing resources. The reaction pathways for the interaction between HSO_5^- and MoS_2 (pristine and polarized) to generate free radicals were investigated by DFT calculations, as shown in Fig. 5. The computational results showed that the reaction between pristine MoS_2 and HSO_5^- to induce the decomposition of HSO_5^- into –OH and –SO_4 moieties was endothermic with a formation energy of 0.721 eV, which was energetically unfavorable. In contrast, the reaction between the S atom edge accumulated with e_{piezo} (compressive strain of −10%) and HSO_5^- to induce the scission of O–O bond was calculated to be exothermic (0.395 eV), suggesting the enhanced activation ability of MoS_2 under strain. This result is

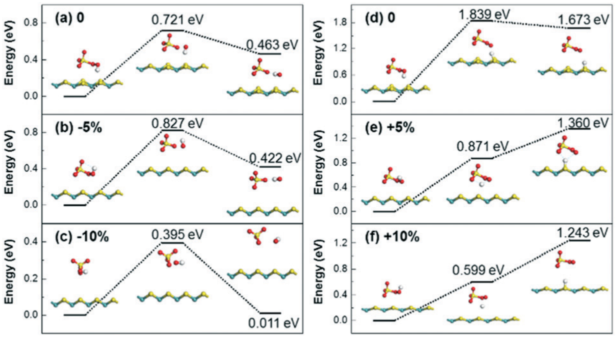

Fig. 5 Reaction pathways for the interaction between HSO_5^- and MoS_2 (pristine and polarized) to generate free radicals under compressive and tensile strain. The formation of the $^{\cdot}OH$ from HSO_5^- in the presence of the strain of MoS_2 in the range of 0 (a), −5% (b) and −10% (c), respectively, while that of the generation of $SO_5^{\cdot-}$ are shown in 0 (d), +5% (e), and +10% (f). The corresponding energies are also listed. Atom color code: sulfur (yellow), molybdenum (cyan), oxygen (red), hydrogen (white).

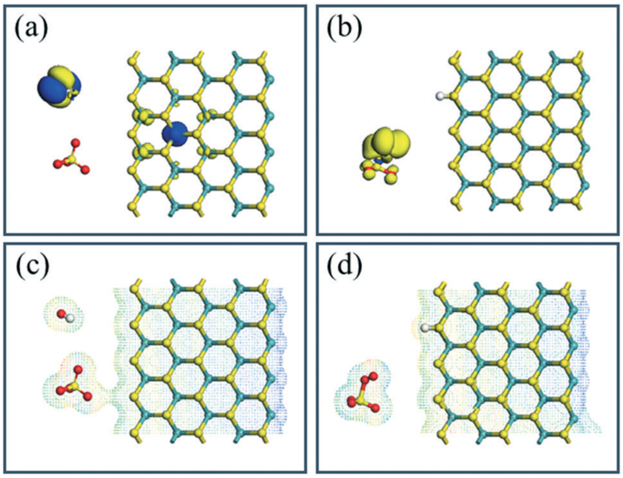

Fig. 6 (a) Spin density of –OH and –SO_4 moieties; (b) spin density of –H and –SO_5 moieties; (c) and (d) COSMO structures corresponding to the spin density in (a) and (b), respectively.

consistent with the band structure at −5% strain. In addition, the activation reaction of HSO_5^- into –OH and $–SO_4$ moieties could efficiently happen when the compressive strain was more than 5%. Furthermore, the electronic spin density of the generated $–SO_5$ and –OH moieties was calculated to determine whether the produced –OH moiety is a free radical, because free radicals typically have characteristic lone-pair electrons, which enable them to be detected by EPR.[48] The spin determination of all the structures during PMS activation are shown in Table S3.† Fig. 6a and c depict the spin density and the water solvation model (COSMO) structure corresponding to the spin density. It can be seen that the produced –OH moiety was $^{\bullet}OH$, which was consistent with the quenching experiments and EPR observations.

Meanwhile, the reaction between pristine MoS_2 and HSO_5^- to induce the decomposition of HSO_5^- into –H and $–SO_5$ moieties was also investigated, as shown in Fig. 5d. It was found that this reaction process was endothermic with an energy barrier as high as 1.839 eV, which was energetically unfavorable. Combined with the result in Fig. 5a, the DFT calculations demonstrated the poor ability of pristine MoS_2 nanosheets for PMS activation, which was in agreement with the experiments. However, once a tensile strain was imposed on MoS_2, the endothermic energy of the reaction was dramatically decreased to 0.871 eV (+5% strain) and 0.599 eV (+10% strain), respectively. Considering that the US vibration used in the experiment would also provide thermal energy, the occurrence of the reaction between PMS and S edge with the accumulated h^+_{piezo} of polarized MoS_2 to generate –H and $–SO_5$ moieties could also be thermodynamically feasible in the US/MoS_2 NFs/PMS system. The reaction became a spontaneous process with the increased strain. Additionally, the produced $–SO_5$ moieties in the cases of the +5% and +10% strains were revealed to be $SO_5^{\bullet-}$ based on the spin density and the COSMO structure (Table S3,† Fig. 6b and d). It has been reported that the reaction of two $SO_5^{\bullet-}$ can form one $SO_4^{\bullet-}$.[4] Therefore, the DFT calculations supported our experimental observation of $SO_4^{\bullet-}$ in the US/MoS_2 NFs/PMS system, and elucidated the possible conversion path of $SO_4^{\bullet-}$ and $^{\bullet}OH$ in the experiment. To conclude, the computational results not only consolidated that the piezoelectric effect in strained MoS_2 NFs enhanced the PMS activation efficiency, but also well interpreted the evolution processes of free radicals in the US/MoS_2 NFs/PMS experimental system at the atomic scale. These findings provide greater understanding of the piezocatalytic activation of persulfate.

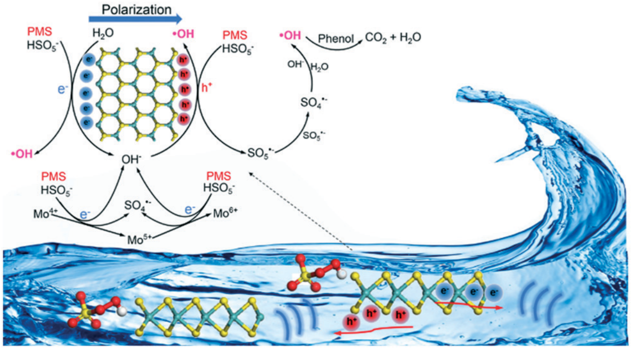

Fig. 7 Piezocatalytic activation mechanisms of PMS over strained MoS_2 NFs for phenol degradation.

According to the above results, the principal reactions that occur in the US/MoS_2 NFs/PMS system toward phenol degradation are proposed in eqn (1)–(11) and the corresponding catalytic mechanism is described in Fig. 7. Under the US vibration, the piezoelectric polarization of MoS_2 NFs is induced and the formed built-in electric field drives the migration of electron and hole pairs to the opposite directions, producing a considerable amount of positively and negatively piezopotential charges on the active edge sites of MoS_2 NFs (eqn (1)).[18,20,49] The e_{piezo} tends to react with HSO_5^- ion to initiate the one-electron reduction reaction (eqn (2)) and to generate $^{\bullet}OH$. Meanwhile, h^+_{piezo} reacts with HSO_5^- ion to produce $SO_5^{\bullet-}$ (eqn (3)) and the combination of two $SO_5^{\bullet-}$ ions leads to the formation of a $SO_4^{\bullet-}$ ion (eqn (4)).[4] Because the collapse of the cavitation bubbles under US vibration can instantaneously produce ultrahigh temperature in the range of 2000–5000 K, a supercritical water zone with higher temperature and pressure is formed in the interfacial region. Therefore, $SO_4^{\bullet-}$ can easily abstract hydrogen atoms from water molecules to produce $^{\bullet}OH$ in the hot region due to the reduced energy barrier under high temperature (eqn (5)).[35,44,50,51] On the other hand, a minority of piezo-induced charges react with water molecules to generate a small amount of $^{\bullet}OH$ (eqn (6) and (7)).[49,52] Additionally, the activation of PMS by MoS_2 itself may also generate a minor amount of $SO_4^{\bullet-}$ (eqn (8) and (9)).[37,38] Finally, phenol molecules are attacked by $^{\bullet}OH$ and thus decomposed into intermediates, and further into CO_2 and H_2O (eqn (10) and (11)).

$$MoS_2\ NFs \xrightarrow{\text{Polarization}} e_{piezo} + h^+_{piezo} \tag{1}$$

$$HSO_5^- + e_{piezo} \rightarrow {}^{\bullet}OH + SO_4^{2-} \tag{2}$$

$$HSO_5^- + h^+_{piezo} \rightarrow H^+ + SO_5^{\bullet-} \tag{3}$$

$$SO_5^{\bullet-} + SO_5^{\bullet-} \rightarrow 2SO_4^{\bullet-} + O_2 \tag{4}$$

$$SO_4^{\bullet-} + H_2O \rightarrow H^+ + SO_4^{2-} + {}^{\bullet}OH \tag{5}$$

$$H_2O + e_{piezo} \rightarrow {}^{\bullet}H + OH^- \tag{6}$$

$$OH^- + h^+_{piezo} \rightarrow {}^{\bullet}OH \tag{7}$$

$$MoS_2 - Mo^{4+} + HSO_5^- \rightarrow MoS_2 - Mo^{5+} + SO_4^{\bullet-} + OH^- \tag{8}$$

$$MoS_2 - Mo^{5+} + HSO_5^- \rightarrow MoS_2 - Mo^{6+} + SO_4^{\bullet-} + OH^- \tag{9}$$

$$\text{Phenol} + {}^{\bullet}OH \rightarrow \text{intermediates} \tag{10}$$

$$\text{Intermediates} + {}^{\bullet}\text{OH} \rightarrow CO_2 + H_2O + \text{inorganic compounds} \quad (11)$$

Stability of the US/MoS$_2$ NFs/PMS system for phenol degradation

In practical wastewater treatment, the stability of piezoelectric catalysts is an important factor to take into consideration. The reusability of MoS$_2$ NFs for the piezocatalytic activation of PMS was assessed for three cycles (Fig. S10a†). The phenol degradation efficiencies by the US/MoS$_2$ NFs/PMS system were 96%, 98%, and 94% in the 1st, 2nd, and 3rd cycles, respectively, revealing the good stability of the MoS$_2$ NFs for piezocatalytic PMS activation. In addition, the XRD patterns of the MoS$_2$ NFs piezocatalyst after the degradation experiment was also examined for comparison (Fig. S10b†). Apparently, a marginal difference in the XRD patterns between the fresh MoS$_2$ NFs and used MoS$_2$ NFs was observed, showing that the crystalline structure of the piezocatalyst barely changed during the catalytic oxidation reaction. Unfortunately, Mo ions have a certain degree of dissolution, and this process should be controlled and optimized in future applications. The TOC removal of phenol by the US/MoS$_2$ NFs/PMS system after a 180 min degradation process was 9.25%, indicating the presence of intermediate products. The degradation intermediates of phenol have been extensively studied in the literature, where it has been reported that, through the hydroxylation of the aromatic ring and the ring opening, phenol can be oxidized into shorter-chain organic acids with lower toxicity, such as maleic acid, oxalic acid, formic acid, acetic, and malonic acid.[53–55] These results suggest that MoS$_2$ NFs are an efficient and stable piezocatalyst for activating PMS to degrade organic pollutants, which promises great potential in applications for water remediation.

Conclusions

In summary, a novel PMS activation technique was demonstrated through coupling piezocatalysis with PMS activation over a MoS$_2$ NFs piezocatalyst to promote phenol degradation. The MoS$_2$ NFs could effectively use the mechanical energy generated by ultrasound to deform, resulting in electron–hole pairs in the piezocatalyst, thereby activating PMS to achieve the removal of pollutants. After coupling the piezoelectric effect of the MoS$_2$ NFs with PMS activation, the degradation efficiency of phenol was greatly improved. $^{\bullet}$OH was suggested to be the primary ROS responsible for phenol oxidation in the US/MoS$_2$ NFs/PMS system according to the quenching tests, while EPR analysis revealed the generation of both $^{\bullet}$OH and $SO_4^{\bullet-}$ in the piezo-activated PS-AOPs system. DFT calculations revealed the mechanisms of the production of free radicals: (i) the HSO_5^- was reduced by the e_{piezo} in the strained MoS$_2$ NFs to form $^{\bullet}$OH and SO_4^{2-}; (ii) the combination of $SO_5^{\bullet-}$ from the interaction between HSO_5^- and h^+_{piezo} in the strained MoS$_2$ NFs generated $SO_4^{\bullet-}$, and subsequently $SO_4^{\bullet-}$ was converted into $^{\bullet}$OH *via* hydrolysis with the assistance of US; (iii) MoS$_2$ NFs acted as a heterogeneous catalyst to activate PMS through the redox cycles of Mo ions. This work provides a potential alternative strategy for environmental restoration using piezoelectric catalysis in the future.

Conflicts of interest

There are no conflicts to declare.

Acknowledgements

This work was supported by the National Natural Science Foundation of China (grant no. 21806024 and 21777033), China Postdoctoral Science Foundation (grant no. 2017M622637), Science and Technology Planning Project of Guangdong Province (grant no. 2017B020216003), Guangdong Natural Science Foundation (grant no. 2020A1515011150) and the Innovation Team Project of Guangdong Provincial Department of Education (grant no. 2017KCXTD012).

Notes and references

1 H. V. Lutze, S. Bircher, I. Rapp, N. Kerlin, R. Bakkour, M. Geisler, C. von Sonntag and T. C. Schmidt, Degradation of chlorotriazine pesticides by sulfate radicals and the influence of organic matter, *Environ. Sci. Technol.*, 2015, **49**, 1673–1680.

2 J. Li, Y. Li, Z. Xiong, G. Yao and B. Lai, The electrochemical advanced oxidation processes coupling of oxidants for organic pollutants degradation: A mini-review, *Chin. Chem. Lett.*, 2019, **30**, 2139–2146.

3 J. Wang and S. Wang, Activation of persulfate (PS) and peroxymonosulfate (PMS) and application for the degradation of emerging contaminants, *Chem. Eng. J.*, 2018, **334**, 1502–1517.

4 F. Ghanbari and M. Moradi, Application of peroxymonosulfate and its activation methods for degradation of environmental organic pollutants: Review, *Chem. Eng. J.*, 2017, **310**, 41–62.

5 L. W. Matzek and K. E. Carter, Activated persulfate for organic chemical degradation: A review, *Chemosphere*, 2016, **151**, 178–188.

6 X. Duan, Z. Ao, H. Zhang, M. Saunders, H. Sun, Z. Shao and S. Wang, Nanodiamonds in sp(2)/sp(3) configuration for radical to nonradical oxidation: Core-shell layer dependence, *Appl. Catal., B*, 2018, **222**, 176–181.

7 C. Nie, Z. Dai, H. Meng, X. Duan, Y. Qin, Y. Zhou, Z. Ao, S. Wang and T. An, Peroxydisulfate activation by positively polarized carbocatalyst for enhanced removal of aqueous organic pollutants, *Water Res.*, 2019, **166**, 115043.

8 C. Nie, Z. Dai, W. Liu, X. Duan, C. Wang, B. Lai, Z. Ao, S. Wang and T. An, Criteria of active sites in nonradical persulfate activation process from integrated experimental and theoretical investigations: boron-nitrogen-co-doped

nanocarbon-mediated peroxydisulfate activation as an example, *Environ. Sci.: Nano*, 2020, **7**, 1899–1911.

9 X. Lei, M. You, F. Pan, M. Liu, P. Yang, D. Xia, Q. Li, Y. Wang and J. Fu, CuFe2O4@GO nanocomposite as an effective and recoverable catalyst of peroxymonosulfate activation for degradation of aqueous dye pollutants, *Chin. Chem. Lett.*, 2019, **30**, 2216–2220.

10 H. Meng, C. Nie, W. Li, X. Duan, B. Lai, Z. Ao, S. Wang and T. An, Insight into the effect of lignocellulosic biomass source on the performance of biochar as persulfate activator for aqueous organic pollutants remediation: Epicarp and mesocarp of citrus peels as examples, *J. Hazard. Mater.*, 2020, **399**, 123043.

11 S. Yang, P. Wang, X. Yang, L. Shan, W. Zhang, X. Shao and R. Niu, Degradation efficiencies of azo dye Acid Orange 7 by the interaction of heat, UV and anions with common oxidants: persulfate, peroxymonosulfate and hydrogen peroxide, *J. Hazard. Mater.*, 2010, **179**, 552–558.

12 K. H. Chu, Y. A. J. Al-Hamadani, C. M. Park, G. Lee, M. Jang, A. Jang, N. Her, A. Son and Y. Yoon, Ultrasonic treatment of endocrine disrupting compounds, pharmaceuticals, and personal care products in water: A review, *Chem. Eng. J.*, 2017, **327**, 629–647.

13 L. W. Matzek and K. E. Carter, Activated persulfate for organic chemical degradation: A review, *Chemosphere*, 2016, **151**, 178–188.

14 H. Lee, H.-I. Kim, S. Weon, W. Choi, Y. S. Hwang, J. Seo, C. Lee and J.-H. Kim, Activation of persulfates by graphitized nanodiamonds for removal of organic compounds, *Environ. Sci. Technol.*, 2016, **50**, 10134–10142.

15 C. Nie, Z. Ao, X. Duan, C. Wang, S. Wang and T. An, Degradation of aniline by electrochemical activation of peroxydisulfate at MWCNT cathode: The proofed concept of nonradical oxidation process, *Chemosphere*, 2018, **206**, 432–438.

16 Z. L. Wang, Progress in piezotronics and piezo-phototronics, *Adv. Mater.*, 2012, **24**, 4632–4646.

17 L. Wang, S. Liu, Z. Wang, Y. Zhou, Y. Qin and Z. L. Wang, Piezotronic effect enhanced photocatalysis in strained anisotropic ZnO/TiO2 nanoplatelets via thermal stress, *ACS Nano*, 2016, **10**, 2636–2643.

18 J. M. Wu, Y.-G. Sun, W.-E. Chang and J.-T. Lee, Piezoelectricity induced water splitting and formation of hydroxyl radical from active edge sites of MoS2 nanoflowers, *Nano Energy*, 2018, **46**, 372–382.

19 Z. Liang, C.-F. Yan, S. Rtimi and J. Bandara, Piezoelectric materials for catalytic/photocatalytic removal of pollutants: Recent advances and outlook, *Appl. Catal., B*, 2019, **241**, 256–269.

20 K.-S. Hong, H. Xu, H. Konishi and X. Li, Piezoelectrochemical effect: A new mechanism for Azo Dye decolorization in aqueous solution through vibrating piezoelectric microfibers, *J. Phys. Chem. C*, 2012, **116**, 13045–13051.

21 R. R. Solis, F. Javier Rivas and M. Tierno, Monopersulfate photocatalysis under 365 nm radiation. Direct oxidation and monopersulfate promoted photocatalysis of the herbicide tembotrione, *J. Environ. Manage.*, 2016, **181**, 385–394.

22 S. Lan, Y. Chen, L. Zeng, H. Ji, W. Liu and M. Zhu, Piezo-activation of peroxymonosulfate for benzothiazole removal in water, *J. Hazard. Mater.*, 2020, **393**, 122448.

23 Y. Feng, L. Ling, Y. Wang, Z. Xu, F. Cao, H. Li and Z. Bian, Engineering spherical lead zirconate titanate to explore the essence of piezo-catalysis, *Nano Energy*, 2017, **40**, 481–486.

24 J. Wu, N. Qin and D. Bao, Effective enhancement of piezocatalytic activity of BaTiO3 nanowires under ultrasonic vibration, *Nano Energy*, 2018, **45**, 44–51.

25 P. Ares, T. Cea, M. Holwill, Y. B. Wang, R. Roldan, F. Guinea, D. V. Andreeva, L. Fumagalli, K. S. Novoselov and C. R. Woods, Piezoelectricity in Monolayer Hexagonal Boron Nitride, *Adv. Mater.*, 2020, **32**, 1905504.

26 W. Wu, L. Wang, Y. Li, F. Zhang, L. Lin, S. Niu, D. Chenet, X. Zhang, Y. Hao, T. F. Heinz, J. Hone and Z. L. Wang, Piezoelectricity of single-atomic-layer MoS2 for energy conversion and piezotronics, *Nature*, 2014, **514**, 470–474.

27 Y. Du, M. Zhou and L. Lei, Role of the intermediates in the degradation of phenolic compounds by Fenton-like process, *J. Hazard. Mater.*, 2006, **136**, 859–865.

28 Y. Wang, H. Sun, H. M. Ang, M. O. Tadé and S. Wang, 3D-hierarchically structured MnO2 for catalytic oxidation of phenol solutions by activation of peroxymonosulfate: Structure dependence and mechanism, *Appl. Catal., B*, 2015, **164**, 159–167.

29 Z. Hu, L. Wang, K. Zhang, J. Wang, F. Cheng, Z. Tao and J. Chen, MoS2 nanoflowers with expanded interlayers as high-performance anodes for sodium-ion batteries, *Angew. Chem., Int. Ed.*, 2014, **53**, 12794–12798.

30 X. Xiong, W. Luo, X. Hu, C. Chen, L. Qie, D. Hou and Y. Huang, Flexible Membranes of MoS2/C Nanofibers by Electrospinning as Binder-Free Anodes for High-Performance Sodium-Ion Batteries, *Sci. Rep.*, 2015, **5**, 9254.

31 J. M. Wu, W. E. Chang, Y. T. Chang and C. K. Chang, Piezo-catalytic effect on the enhancement of the ultra-high degradation activity in the dark by single- and few-layers MoS2 nanoflowers, *Adv. Mater.*, 2016, **28**, 3718–3725.

32 C.-B. Ma, X. Qi, B. Chen, S. Bao, Z. Yin, X.-J. Wu, Z. Luo, J. Wei, H.-L. Zhang and H. Zhang, MoS2 nanoflower-decorated reduced graphene oxide paper for high-performance hydrogen evolution reaction, *Nanoscale*, 2014, **6**, 5624–5629.

33 K.-J. Huang, Y.-J. Liu, Y.-M. Liu and L.-L. Wang, Molybdenum disulfide nanoflower-chitosan-Au nanoparticles composites based electrochemical sensing platform for bisphenol A determination, *J. Hazard. Mater.*, 2014, **276**, 207–215.

34 X. Li, T. Li, Y. Ma, Q. Wei, W. Qiu, H. Guo, X. Shi, P. Zhang, A. M. Asiri, L. Chen, B. Tang and X. Sun, Boosted electrocatalytic N-2 reduction to NH3 by defect-rich MoS2 nanoflower, *Adv. Energy Mater.*, 2018, **8**, 1801357.

35 R. Yin, W. Guo, H. Wang, J. Du, X. Zhou, Q. Wu, H. Zheng, J. Chang and N. Ren, Enhanced peroxymonosulfate activation

for sulfamethazine degradation by ultrasound irradiation: Performances and mechanisms, *Chem. Eng. J.*, 2018, **335**, 145–153.

36 S. Wang and N. Zhou, Removal of carbamazepine from aqueous solution using sono-activated persulfate process, *Ultrason. Sonochem.*, 2016, **29**, 156–162.

37 B. Sheng, F. Yang, Y. Wang, Z. Wang, Q. Li, Y. Guo, X. Lou and J. Liu, Pivotal roles of MoS2 in boosting catalytic degradation of aqueous organic pollutants by Fe(II)/PMS, *Chem. Eng. J.*, 2019, **375**, 121989.

38 H. Zhou, L. Lai, Y. Wan, Y. He, G. Yao and B. Lai, Molybdenum disulfide (MoS2): A versatile activator of both peroxymonosulfate and persulfate for the degradation of carbamazepine, *Chem. Eng. J.*, 2020, **384**, 123264.

39 X. Duan, C. Su, L. Zhou, H. Sun, A. Suvorova, T. Odedairo, Z. Zhu, Z. Shao and S. Wang, Surface controlled generation of reactive radicals from persulfate by carbocatalysis on nanodiamonds, *Appl. Catal., B*, 2016, **194**, 7–15.

40 J. Wei, X. Li, Q. Yang, Y. Wu, X. Huang, Z. Tao, Q. Xu, X. Zhu and D. Wang, Sulfate radical-mediated degradation of phenol and methylene blue by manganese oxide octahedral molecular sieve (OMS-2) activation of peroxymonosulfate, *Environ. Sci. Pollut. Res.*, 2019, **26**, 12963–12974.

41 P. Neta, R. E. Huie and A. B. Ross, Rate constants for reactions of inorganic radicals in aqueous solution, *J. Phys. Chem. Ref. Data*, 1988, **17**, 1027–1284.

42 G. V. Buxton, C. L. Greenstock, W. P. Helman and A. B. Ross, Critical review of rate constants for reactions of hydrated electrons, hydrogen atoms and hydroxyl radicals (·OH/·O−) in Aqueous Solution, *J. Phys. Chem. Ref. Data*, 1988, **17**, 513–886.

43 W.-D. Oh, Z. Dong and T.-T. Lim, Generation of sulfate radical through heterogeneous catalysis for organic contaminants removal: Current development, challenges and prospects, *Appl. Catal., B*, 2016, **194**, 169–201.

44 Z. Wei, F. A. Villamena and L. K. Weavers, Kinetics and mechanism of ultrasonic activation of persulfate: An in situ EPR spin trapping study, *Environ. Sci. Technol.*, 2017, **51**, 3410–3417.

45 X. Wang, J. Song, J. Liu and Z. L. Wang, Direct-current nanogenerator driven by ultrasonic waves, *Science*, 2007, **316**, 102–105.

46 G. C. Yoon, K.-S. Shin, M. K. Gupta, K. Y. Lee, J.-H. Lee, Z. L. Wang and S.-W. Kim, High-performance hybrid cell based on an organic photovoltaic device and a direct current piezoelectric nanogenerator, *Nano Energy*, 2015, **12**, 547–555.

47 B. Jing, Z. Ao, Z. Teng, C. Wang, J. Yi and T. An, Density functional theory study on the effects of oxygen groups on band gap tuning of graphitic carbon nitrides for possible photocatalytic applications, *Sustainable Mater. Technol.*, 2018, **16**, 12–22.

48 Y. Wang, W. Yang, X. Chen, J. Wang and Y. Zhu, Photocatalytic activity enhancement of core-shell structure g-C3N4@TiO2 via controlled ultrathin g-C3N4 layer, *Appl. Catal., B*, 2018, **220**, 337–347.

49 S. Lan, J. Feng, Y. Xiong, S. Tian, S. Liu and L. Kong, Performance and mechanism of piezo-catalytic degradation of 4-chlorophenol: finding of effective piezo-dechlorination, *Environ. Sci. Technol.*, 2017, **51**, 6560–6569.

50 M. Ahmad, A. L. Teel and R. J. Watts, Mechanism of persulfate activation by phenols, *Environ. Sci. Technol.*, 2013, **47**, 5864–5871.

51 X. Duan, S. Indrawirawan, J. Kang, W. Tian, H. Zhang, H. Sun and S. Wang, Temperature-dependent evolution of hydroxyl radicals from peroxymonosulfate activation over nitrogen-modified carbon nanotubes, *Sustainable Mater. Technol.*, 2018, **18**, 8.

52 X. Xu, Z. Wu, L. Xiao, Y. Jia, J. Ma, F. Wang, L. Wang, M. Wang and H. Huang, Strong piezo-electro-chemical effect of piezoelectric BaTiO3 nanofibers for vibration-catalysis, *J. Alloys Compd.*, 2018, **762**, 915–921.

53 J. A. Zazo, J. A. Casas, A. F. Mohedano, M. A. Gilarranz and J. J. Rodriguez, Chemical pathway and kinetics of phenol oxidation by Fenton's reagent, *Environ. Sci. Technol.*, 2005, **39**, 9295–9302.

54 G. X. Huang, C. Y. Wang, C. W. Yang, P. C. Guo and H. Q. Yu, Degradation of Bisphenol A by Peroxymonosulfate Catalytically Activated with Mn1.8Fe1.2O4 Nanospheres: Synergism between Mn and Fe, *Environ. Sci. Technol.*, 2017, **51**, 12611–12618.

55 E. Mousset, L. Frunzo, G. Esposito, E. D. V. Hullebusch, N. Oturan and M. A. Oturan, A complete phenol oxidation pathway obtained during electro-Fenton treatment and validated by a kinetic model study, *Appl. Catal., B*, 2016, **180**, 189–198.